BIOPHYSICS

Entropic effects enable life at extreme temperatures

Young Hun Kim[1]*, Geoffray Leriche[1]*, Karthik Diraviyam[2], Takaoki Koyanagi[1], Kaifu Gao[3], David Onofrei[4], Joseph Patterson[1], Anirvan Guha[5], Nathan Gianneschi[6], Gregory P. Holland[4], Michael K. Gilson[3], Michael Mayer[5], David Sept[2], Jerry Yang[1†]

Maintaining membrane integrity is a challenge at extreme temperatures. Biochemical synthesis of membrane-spanning lipids is one adaptation that organisms such as thermophilic archaea have evolved to meet this challenge and preserve vital cellular function at high temperatures. The molecular-level details of how these tethered lipids affect membrane dynamics and function, however, remain unclear. Using synthetic monolayer-forming lipids with transmembrane tethers, here, we reveal that lipid tethering makes membrane permeation an entropically controlled process that helps to limit membrane leakage at elevated temperatures relative to bilayer-forming lipid membranes. All-atom molecular dynamics simulations support a view that permeation through membranes made of tethered lipids reduces the torsional entropy of the lipids and leads to tighter lipid packing, providing a molecular interpretation for the increased transition-state entropy of leakage.

INTRODUCTION

Thermophilic archaea can live at temperatures exceeding 90°C (*1*). Among other adaptations, these organisms generate lipid membranes with unique structural features that help retain their barrier function in these extreme environments (*2*–*4*). Specifically, archaeal lipids (*5*) have ether linkages between their polar head groups and lipid tails, rather than the more labile ester groups found in eukaryotic and prokaryotic lipid membranes (*6*). In addition, archaea lipids typically contain highly branched lipid tails, unlike non-archaeal lipids; these phytanyl chains improve the packing of the lipids (*7*) while simultaneously maintaining the lipids in a liquid phase (as opposed to a gel phase) over a wide range of temperatures (*6*). Therefore, "heat-tolerant" archaeal lipids can be used at both high and low temperatures because of their liquid crystalline phase and low permeability at a wide range of temperatures. Additional structural elements (*8*, *9*) commonly found in archaeal lipids, in particular lipid tethering (*10*), may also impart important functional characteristics in archaeal membranes; however, the relationship between these structural features and temperature-dependent membrane integrity remains poorly understood.

One of the most striking features of membranes from thermophilic archaea is that, unlike eukaryotic cells, they contain bipolar tethered lipids—that is, fully membrane-spanning lipids containing two polar head groups and covalently linked lipid tails that form monolayer membranes—as opposed to the monopolar phospholipid bilayers of eukaryotic cells. It has been shown that the fraction of bipolar tethered lipids in archaeal membranes increases with higher temperatures (Fig. 1) (*11*–*14*), leading to speculation that molecular tethering of lipids plays a role in regulating flexibility and fluidity of archaeal membranes at elevated temperatures (*13*). However, due to the complexity of mixtures of natural lipids present in membrane extracts (*3*) and the lack of available synthetic bipolar tethered lipids, there are few reported studies that examine the effect of lipid tethering on membrane function at elevated temperatures. For instance, previous reports show that tethering of synthetic lipids decreases membrane leakage of small molecules and ions at high temperatures compared to untethered lipids (*3*, *15*, *16*). While these reports provided important first steps toward examining the properties of membranes containing tethered lipids, their use of lipid mixtures or lack of control of relevant lipid characteristics such as phase transition temperatures, distribution of sizes of liposomes, or lamellarity makes it difficult to conclude any mechanistic relationship between the structure of bipolar tethered lipids and membrane leakage profiles at different temperatures. Here, we report a controlled permeation analysis of temperature-dependent liposome leakage for three synthetic bipolar tethered or monopolar untethered lipids that, in combination with molecular dynamics (MD) simulations, provides a molecular description for the effect of lipid tethering on membrane leakage at temperatures ranging from 22° to 70°C.

RESULTS

Lipid tethering reduces temperature-dependent membrane leakage

To examine the effect of lipid tethering on membrane leakage as a function of temperature, we encapsulated carboxyfluorescein (CF) at self-quenching concentration (100 mM) in three different thermostable (fig. S1G) liposomal formulations, composed of pure synthetic lipids with ether linkages (T32, T36, and U16; Fig. 2A and fig. S1A), and used fluorescence intensity measurements to monitor the efflux of CF at temperatures of 22°, 37°, 50°, 60°, and 70°C over the course of 8 hours. Here, T32 is a hemicyclic bipolar lipid with a tethered chain length of 32 methylene units; monopolar U16 lipid is effectively T32 cut in half at the C16/C17 bond of the tethered lipid chain, and T36 is the same as T32 except that the tethered chain is four methylene groups longer and, thus, makes it possible to probe the effect of a longer tether on membrane permeation. We used CF in these elevated temperature studies because we found that the rate of CF leakage could be readily and reproducibly monitored spectroscopically across all temperatures. Figure 2 (B to D) plots the time-dependent efflux of CF from unilamellar liposomes with a diameter of ~80 nm (figs. S1, B to D, and S2A), composed of each of the three pure lipids, as a function of temperature.

[1]Department of Chemistry and Biochemistry, University of California, San Diego, La Jolla, CA 92093, USA. [2]Department of Biomedical Engineering, Center for Computational Medicine and Bioinformatics, University of Michigan, Ann Arbor, MI 48109, USA. [3]Skaggs School of Pharmacy and Pharmaceutical Sciences, University of California, San Diego, La Jolla, CA 92093, USA. [4]Department of Chemistry and Biochemistry, San Diego State University, San Diego, CA 92182, USA. [5]Adolphe Merkle Institute, University of Fribourg, Chemin des Verdiers 4, Fribourg, Switzerland. [6]Departments of Chemistry, Materials Science and Engineering, and Biomedical Engineering, Northwestern University, Evanston, IL 60208, USA.
*These authors contributed equally to this work.
†Corresponding author. Email: jerryyang@ucsd.edu

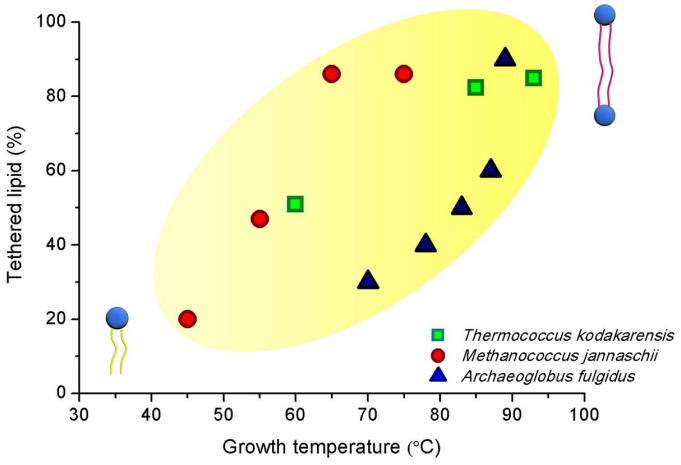

Fig. 1. Correlation between the abundance of tethered lipids and growth temperature in archaea. The percentage of tethered lipids in the membranes of three different archaea organisms was found to increase with increasing external growth temperature (*12*–*14*).

While the rate constants (and permeability coefficients) for CF leakage out of liposomes from all three lipids increase with increasing temperature (Fig. 2A and fig. S3), liposomes composed of T32 and T36 showed a reduced dependence on temperature compared to U16. The only difference between these leakage experiments was the presence of the tether in the lipid, which has a substantial influence on the temperature dependence of CF leakage. A similar trend in CF leakage rates was observed when using ~200-nm-diameter liposomes (figs. S2B and S4), demonstrating that the observed effect of tethering persists at reduced membrane curvature.

Entropic effects from lipid tethering reduces permeation at elevated temperatures

To gain mechanistic insight into the temperature dependence of leakage, we performed a Eyring-Polanyi kinetic analysis of the leakage data (*17*). This analysis reveals the contributions of the enthalpy and entropy of activation for CF leakage from liposomes. A key finding is that the activation enthalpy and entropy for CF leakage from the bipolar tethered T32 and T36 lipids are significantly different ($P < 0.0001$) from those of the monopolar untethered U16 lipid (Fig. 2E). Specifically, tethering reduces (makes less positive) the enthalpy of activation ($\Delta H^{\ddagger}$) of CF leakage by 3.6 to 4.7 kcal mol^{-1} (Fig. 2E), which on its own would lead to increased leakage. However, tethering also decreases (makes more negative) the entropy of activation ($\Delta S^{\ddagger}$) of CF leakage by 12 to 16 cal mol^{-1} K^{-1}, and this drop in the activation entropy leads to greater resistance of the tethered lipids to leakage at high temperature. Thus, the larger activation entropy of leakage through membranes of the tethered lipids leads to an increasing Gibbs free energy of activation ($\Delta G^{\ddagger}$) of CF leakage as temperature increases, rendering liposomes composed of bipolar tethered lipids more resistant to changes in leakage rates at temperatures in the range of 22° to 70°C compared to monopolar untethered lipids (Fig. 2F).

Comparison of CF leakage from liposomes with diameters of ~80 or ~200 nm revealed that the liposome size, and hence membrane curvature, influences the magnitude of $\Delta H^{\ddagger}$ and $\Delta S^{\ddagger}$ for CF leakage (Fig. 2E), but the differences in thermodynamic values ($\Delta\Delta H^{\ddagger}$ and $\Delta\Delta S^{\ddagger}$) between tethered and untethered lipids are essentially independent of liposome diameter (Fig. 2, G and H). Additionally, increasing the length of the tether by four methylene groups from T32 to T36 does not affect the temperature-dependent kinetics of CF leakage, suggesting that the effects on membrane structure as a result of extending the length of the lipid tether do not play a dominant role in temperature-dependent leakage.

MD simulations reveal that reduced local diffusion of tethered lipids correlates with reduced permeation

To gain insight at the microscopic level into the effects of tethering on permeation, we performed MD simulations of membranes constructed from each of the three lipids (U16, T32, and T36). In these simulations, all three lipids formed stable membranes at 300, 315, and 330 K (fig. S5), and the results provided estimates for parameters such as membrane thickness, bending stiffness, lateral and self-diffusion constants of lipids, average area per lipid, and variance in area per lipid at these different temperatures. To test the validity of the simulations, we compared the experimental and calculated values for the thickness of the membranes (Fig. 3A and fig. S6) and the rank order of the lateral diffusion (*10*) between the lipids (Fig. 3B and figs. S1E and S7) at 300 K. These values were consistent between calculations and experimental measurements, which suggest that the MD simulations represent the lipids and membranes under investigation well.

We conducted simulations at different temperatures to provide insight into the effects of temperature on lipid dynamics. Previous studies carried out by Matsuno *et al.* (*13*) with extracted archaeal lipids suggest that lipid tethering influences membrane flexibility, while previous simulations show no correlation between bending stiffness and lipid tethering at 300 K (*10*). Nagle and colleagues also previously reported computational results showing that permeation correlates with variance in lipid area (*18*) or area per lipid with bilayer-forming lipids (*19*). The present MD simulations of U16, T32, and T36 show that both the variance in lipid area and area per lipid increase with increasing temperature, as expected (fig. S8), and that these two calculated parameters are highly correlated with each other (Pearson r correlation = 0.94, $P < 0.001$; fig. S9) across all three lipids at all temperatures. While the MD simulations support the idea that T32 and T36 exhibit a smaller variance in lipid area at all temperatures compared to U16 (which suggests that lipid tethering leads to tighter lipid packing), we did not find a strong correlation between the experimental leakage rates of CF obtained at different temperatures and the calculated variance in area per lipid (Pearson r correlation = 0.63, $P = 0.07$; Fig. 3C) or area per lipid (Pearson r correlation = 0.65, $P = 0.06$; fig. S9) at 22°, 37°, and 60°C.

To examine whether any other calculated parameters of the lipids could be predictive of leakage properties for this set of lipids, we examined the correlation between observed leakage rates at different temperatures and the lateral (long-range) diffusion (Pearson r correlation = 0.87, $P = 0.002$; Fig. 3D) and self (local) diffusion (Pearson r correlation = 0.98, $P < 0.0001$; Fig. 3E) for all three synthetic lipids at three different temperatures (300, 315, and 330 K). Here, the Pearson correlation coefficients (r) reveal that the lipid self-diffusion was the better parameter for predicting permeability in this set of lipids.

CF in the membrane introduces a stronger reduction in torsional entropy in tethered over untethered lipids

The experimental leakage studies show that tethering increases the entropic penalty for passage of CF through the membrane and thus reduces permeation at elevated temperature. We speculated that the entropy differences between tethered and untethered lipids might reflect, at least in part, differences in how the presence of CF into the membrane influences the chain entropy of the lipids. We used MD

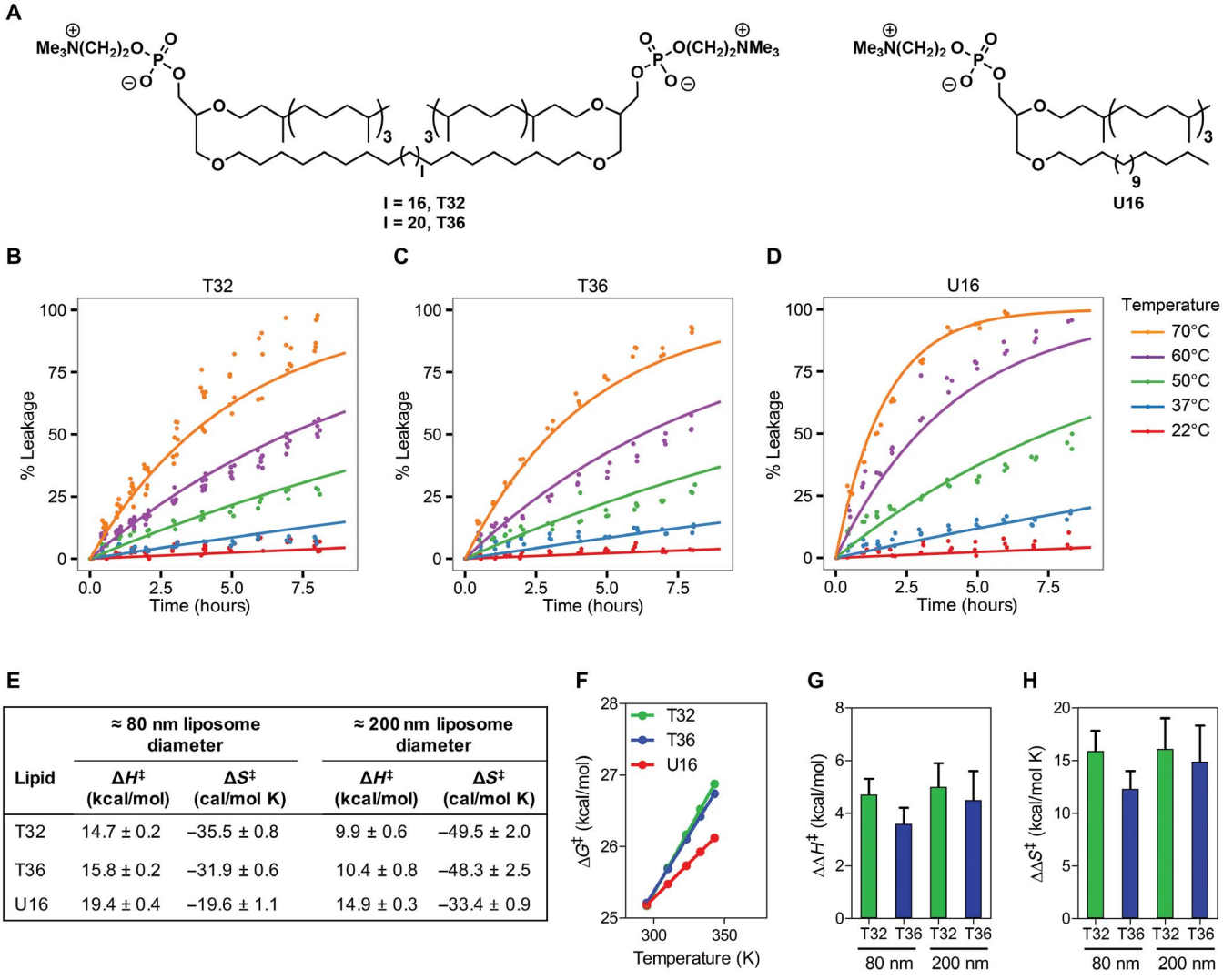

Lipid	≈ 80 nm liposome diameter		≈ 200 nm liposome diameter	
	$\Delta H^{\ddagger}$ (kcal/mol)	$\Delta S^{\ddagger}$ (cal/mol K)	$\Delta H^{\ddagger}$ (kcal/mol)	$\Delta S^{\ddagger}$ (cal/mol K)
T32	14.7 ± 0.2	−35.5 ± 0.8	9.9 ± 0.6	−49.5 ± 2.0
T36	15.8 ± 0.2	−31.9 ± 0.6	10.4 ± 0.8	−48.3 ± 2.5
U16	19.4 ± 0.4	−19.6 ± 1.1	14.9 ± 0.3	−33.4 ± 0.9

Fig. 2. Kinetic analysis of leakage of encapsulated CF from liposomes. (**A**) Structures of monolayer-forming tethered lipids T32 and T36 and bilayer-forming untethered lipid U16. (**B** to **D**) Temperature-dependent CF release profile from liposomes prepared from T32 (B), T36 (C), and U16 (D). Data points show replicate results; solid curves are global fits to rate theory across all of the data in each graph simultaneously (see Materials and Methods). (**E**) Calculated enthalpy ($\Delta H^{\ddagger}$) and entropy ($\Delta S^{\ddagger}$) of activation for encapsulated CF leakage from liposomes using Eyring equation (see the "Kinetic analysis" section). Thermodynamic parameters were calculated using replicates from two separate liposome preparations with different diameters (~80 and ~200 nm). (**F**) Effect of temperature on Gibbs free energy of activation for CF leakage through 80-nm liposomes. Gibbs free energy was calculated at different temperature (22°, 37°, 50°, 60°, and 70°C) using the Gibbs fundamental equation ($\Delta G^{\ddagger} = \Delta H^{\ddagger} - T\Delta S^{\ddagger}$). (**G**) Change in enthalpy ($\Delta\Delta H^{\ddagger}$) for T32 (green) and T36 (blue) compared to $\Delta H^{\ddagger}$ obtained for U16. Student's *t* test revealed no significant difference in $\Delta H^{\ddagger}$ between the two tethered lipids and between the data from different liposome diameters (and, hence, membrane curvature). (**H**) Change in entropy ($\Delta\Delta S^{\ddagger}$) for T32 (green) and T36 (blue) compared to $\Delta S^{\ddagger}$ obtained for U16.

simulations to test this idea, examining changes in the first-order approximation of the chain entropy (S^1) (*20*), when CF is situated partway through one leaflet of a membrane consisting of bipolar tethered lipid T32 or of monopolar untethered lipid U16, as depicted in a sample snapshot from one simulation in Fig. 4A.

The baseline torsional entropy in the absence of CF (Fig. 4, B and C, dashed lines) is substantially lower for the bipolar tethered lipids (Fig. 4, B and C, green) than for the monopolar untethered lipids (Fig. 4, B and C, red), as may be expected due to the conformational constraint imposed by tethering. The difference is greater for the tethered chain (Fig. 4B) than for the phytanyl chain (Fig. 4C). When CF is inserted into the membrane, there is minimal change in the torsional entropy of the monopolar untethered lipids (Fig. 4, B and C, solid versus dashed red lines). However, there is a noticeable drop in entropy for the bipolar tethered lipids (Fig. 4, B and C, solid versus dashed green lines), with the largest reduction in torsional entropy occurring at carbon atoms near the center of the membrane. These effects are larger for the methylene chains than for the phytanyl chains, which are not tethered in either T32 or U16 (Fig. 4D). The entropies provided are per lipid, averaged over all lipids in the simulation (64 for the tethered and 128 for the untethered), so the net effect across all lipids in the membrane is substantial.

Although the CF is held in the top half of the membrane for these simulations (Fig. 4A), the changes in entropy are similar between the top and bottom membrane leaflets, as evident from the symmetry of the perturbations around the central carbon torsion (torsion on carbon 13 in Fig. 4, B and C) and from the similarity of the "top" and "bottom"

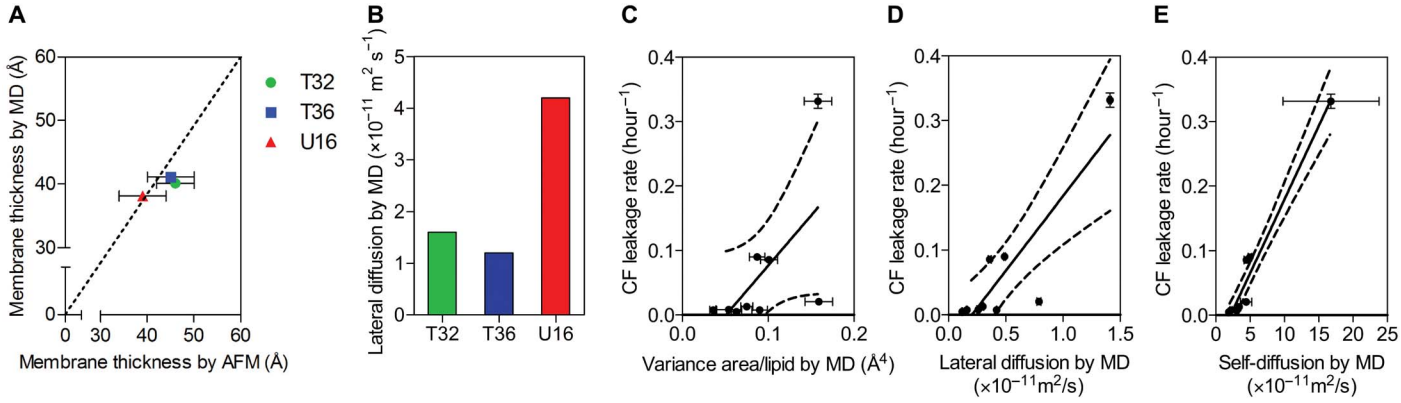

Fig. 3. Computational modeling of bilayer and monolayer membranes. (**A**) Correlation between membrane thickness measured experimentally by atomic force microscopy (AFM) and MD simulations. (**B**) Lateral diffusion coefficient of lipids in the membrane determined by MD simulation. (**C**) Correlation between variance in area per lipid determined by MD at different temperatures and experimental CF leakage rates obtained at different temperatures (Pearson *r* correlation = 0.63, $P = 0.07$). The dashed lines represent the 95% confidence band of the best-fit line. (**D**) Correlation between lipid lateral diffusion determined by MD and experimental CF leakage rates at different temperatures (Pearson *r* correlation = 0.87, $P = 0.002$). The dashed lines represent the 95% confidence band of the best-fit line. (**E**) Correlation between lipid self-diffusion determined by MD and experimental CF leakage rates at different temperatures (Pearson *r* correlation = 0.98, $P < 0.0001$). The dashed lines represent the 95% confidence band of the best-fit line.

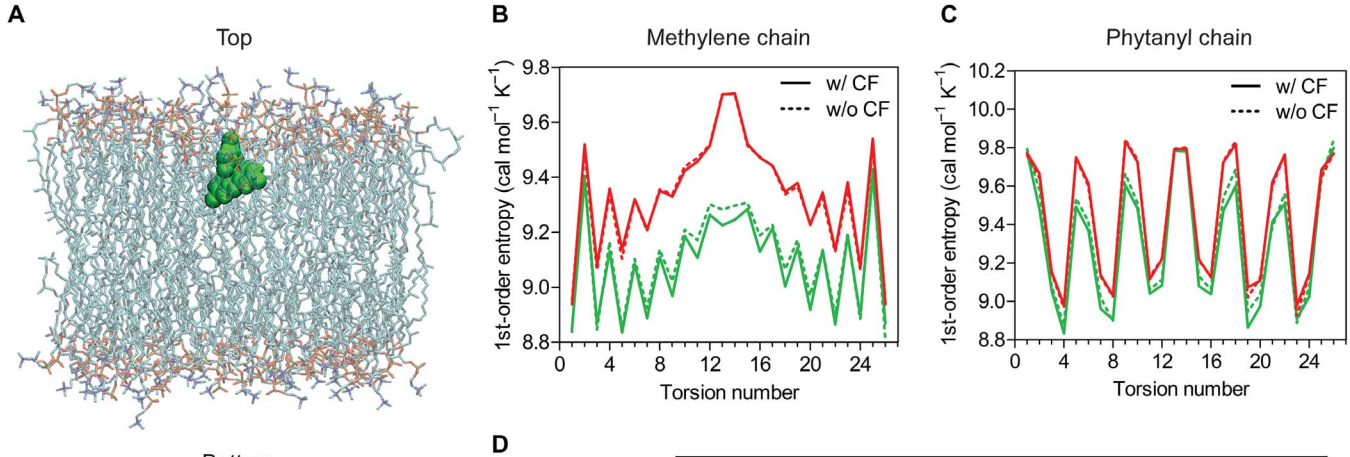

D

	Net effect of the presence of CF on S^1 (cal mol^{-1} K^{-1})			
	T32		U16	
	Methylene chain	Phytanyl chain	Methylene chain	Phytanyl chain
Top leaflet	−0.80	−0.46	0.09	0.05
Bottom leaflet	−0.71	−0.44	0.25	0.15
Total	−1.51	−0.89	0.34	0.20

Fig. 4. First-order entropy of lipid torsions. (**A** to **D**) Entropy analysis based on MD simulations with AMBER 14 (*34*) using GAFF (*35*) and Lipid14 (*36*) parameters, with TIP3P water, of membranes with and without CF restrained at a target depth in one leaflet in the presence of 150 mM KCl. (A) Simulation snapshot of CF restrained in the T32 monolayer membrane (100 ns, 300 K, 64 lipids). (B and C) First-order entropy of lipid torsions as a function of torsion position, where torsion 1 is at the top of the membrane and torsion 26 is at the bottom (A). Results are shown here for the unbranched methylene chain (B) and phytanyl chain (C) of each lipid. Red, untethered (U16) lipids; green, tethered (T32) lipids; solid lines, CF present in the membrane; dashed lines, CF absent from the membrane. The first-order entropy reported for each torsion is a per lipid average over all 64 instances of the torsion in the 64 lipid molecules of the tethered membrane simulations or the 128 lipid molecules of the untethered membrane simulations. (D) Effect of the presence of CF in the membrane on the first-order torsional entropy (in cal mol^{-1} K^{-1}) per lipid of the simulated T32 and U16 lipid membranes, partitioned by lipid chain and bilayer leaflet (top versus bottom).

computed changes in entropy provided in Fig. 4D. Thus, in the tethered case, CF's interactions with the top half of the membrane propagate to the lower half, amplifying the entropic penalty for permeation, while in the untethered case there is no noticeable effect in either leaflet.

DISCUSSION

We demonstrate that lipid tethering significantly increases the entropic barrier for membrane permeation of CF and, accordingly, reduces membrane permeability at elevated temperatures relative to untethered lipids. Further analyses by MD simulations offer a possible explanation for this observation, namely, that the bipolar tethered lipids lose more torsional entropy than do monopolar untethered lipids when CF enters the membrane. Evidently, the addition of CF synergizes with the baseline conformational restrictions imposed by the tethers, leading to increased ordering and lower entropy. The experimental observation of a reduced enthalpic barrier may be more difficult to understand, but it is interesting to speculate about a possible analogy

with hydrophobic solvation. When a small hydrophobic molecule is placed in water, the water molecules at its surface respond by forming cage-like, hydrogen-bonded structures characterized by low entropy and low enthalpy. Placing CF into the membrane may similarly cause the tethered lipids to adopt well-packed structures with favorable lipid-lipid interactions (low enthalpy) and increased ordering (low entropy). At the same time, it should be noted that there are many other entropic and enthalpic differences between tethered and untethered lipids that could contribute to the overall effects observed experimentally. These contributions could arise, e.g., from differences in translational and orientational entropy of the lipids, differences in orientational entropy of the CF molecule in the membrane, and differences in the correlations among the various degrees of freedom.

Simulations showed no significant correlation between tethering and membrane flexibility (estimated by bending stiffness) (*10*), as had been proposed by others (*13*). However, in accord with results from fluorescence recovery after photobleaching experiments (fig. S1E), the present MD simulations support a significant effect of lipid tethering on the viscosity of the membrane, indicated by the diffusion coefficients of the lipids. Given that membrane viscosity is thought to be an important determinant of permeability (*21*), and that we find that entropy plays an important role in the permeability of bipolar tethered versus monopolar untethered lipid membranes, it is of interest that the diffusion constant of molecules in a liquid is expected to correlate with the partial molar entropy (*22*–*24*). Intuitively, more freedom of motion corresponds to both higher entropy and higher mobility. Similar considerations may apply in the context of a membrane.

In conclusion, this study reveals a fundamental principle for maintaining membrane integrity at elevated temperatures. Namely, to render membranes resistant to leakage at elevated temperatures, it is helpful for the free energy barrier of molecular leakage to include a large entropy of activation. Lipid tethering is one molecular strategy toward achieving this goal.

MATERIALS AND METHODS

General information

Dynamic light scattering (DLS) measurements were performed on a Wyatt DynaPro NanoStar (Wyatt Technology, Santa Barbara, CA) instrument using a disposable cuvette (Eppendorf UVette, 220 to 1600 nm), and data were processed using Wyatt DYNAMICS V7 software. Each analysis involved an average of 10 measurements. The data were exported for final plotting using GraphPad Prism 5 (GraphPad Software Inc., La Jolla, CA).

Absorbance measurements were taken on a PerkinElmer EnSpire multimode plate reader. Untreated Corning 96-well half area black flat bottom polystyrene microplates were used (ref. 3694).

Lipid design and synthesis

As opposed to natural archaeal tethered lipids, which typically contain two transmembrane tethers to form a C-40 macrocyclic lipid (*5*), we synthesized and studied bipolar hemi-macrocyclic lipids (*5*) containing a single transmembrane tether between lipid tails; these are synthetically more accessible on the gram scale than fully macrocyclic archaeal lipids (*25*). Specifically, we generated three lipids that all contained a phytanyl acyl chain, an ether linkage to a glycerol, and a phosphocholine head group (fig. S1A). We chose phosphocholine as a head group to increase the probability of forming stable liposomes (*26*). We chose ether linkages to match the ether linkages that are found in archaea, which increase the chemical (i.e., hydrolytic) stability of lipids (*6*). We incorporated an untethered phytanyl acyl chain (as opposed to a saturated hydrocarbon chain without methyl groups) into all lipids to reduce the probability of a phase transition in the temperature range of interest (*6*) and to avoid phase transition–induced leakage (*27*–*29*). This design made it possible to generate lipids T32, T36, and U16 in ~10 synthetic steps, as previously described (*10*).

Liposome preparation

We prepared a liposome solution (10 mg/ml) by first dissolving 5 mg of lipid of interest into a 5-ml round bottom flask in a dichloromethane/MeOH (7:3) solution. A thin lipid film was achieved by evaporating the solvent using a rotary evaporator (Buchi RE-111) and then by drying further with a high-vacuum pump (Welch 1402) for 4 hours. The thin lipid film was then hydrated at 10 mg/ml in either 10 mM Hepes buffer (150 mM KCl, pH 7.0), phosphate-buffered saline (PBS) (1×, pH 7.4), or a solution of PBS containing 100 mM CF by vortexing the solution for 30 s, followed by sonication in a water bath sonicator (Branson 2510) for 30 min. After sonication, the lipid mixture underwent five freeze-thaw cycles that consisted of 2 min at −78°C, followed by 2 min at 50°C. The liposomal suspension was then successively extruded (Avanti Mini Extruder) through 400- and 200-nm polycarbonate membranes (51 times for each membrane) to generate ~200-nm-diameter liposomes. Smaller liposomes (~80 nm diameter) were produced using additional extrusion with 100- and 50-nm polycarbonate membranes (51 times for each membrane). Liposome radii are shown in fig. S2. For CF-encapsulated liposomes, free CF was removed by gel filtration through a Sephadex G-100 column eluted with PBS (1×, pH 7.4), and the lipid solution was then stored at 4°C in a Protein LoBind Eppendorf tube.

Cryo–electron microscopy imaging of liposomes

We applied 5 μl of liposomes in PBS (2 mg/ml, ~80 nm diameter by DLS) to a holey grid, which had been previously treated by glow discharged in an oxygen plasma chamber. The cryo–electron microscopy (EM) sample was vitrified using liquid ethane as the cryogen. The frozen sample was transferred into a precooled cryo-transfer holder to maintain a low temperature. The image was acquired on a FEI Tecnai G2 Sphera microscope operated at 200 keV using a Gatan UltraScan 1000 UHS 4 MP charge-coupled device camera. All three lipids (U16, T32, and T36) can form mostly unilamellar liposomes by lipid film hydration and extrusion through polycarbonate membranes (fig. S1, B to D).

Differential scanning calorimetry

Suspensions of liposomes were prepared by sonication of lipid films for 30 min in ultrapure water. All liposome samples contained a final concentration of ~5% lipid by weight. Differential scanning calorimetry (DSC) experiments were performed in duplicate using a Thermal Analysis Q2000 DSC. Each experiment involved a 1°C/min ramp from 0° to 80°C under dry helium at 50 ml/min. TA Universal Analysis was used to extract the T_m for these samples. DSC experiments revealed that all three lipids do not undergo a phase transition in the temperature range of 0° to 80°C (fig. S1F).

Measurement of membrane thickness by atomic force microscopy

Multilamellar vesicles were first prepared by hydration of a lipid film (10 mg/ml) in Hepes buffer, followed by incubation at 50°C for

30 min. Liposomal suspensions were then sonicated for 5 min and added to a mica substrate. Excess of liposomes was removed after 1 hour, and the mica surfaces were rinsed 10 times with a 150 mM KCl solution. Samples were imaged using a multimode atomic force microscope with a NanoScope IV controller (Bruker, Santa Barbara, CA) (fig. S6). The tapping mode images were acquired using silicon nitride cantilever tips submerged in buffer. A resonance frequency of ~8 kHz and drive amplitude under 100 mV were used (Asylum Research, Santa Barbara, CA). NanoScope software was used for depth analysis to estimate the height of the lipid membranes.

Thermal stability of liposomes

To a glass vial, 0.2 ml of each liposome suspension (~200 nm diameter, prepared in Hepes) was added into 1.8 ml of Hepes buffer. The glass vial was sealed with parafilm to prevent evaporation, and the liposome solutions were incubated at 75°C. For each time point (t = 0 and 6 hours), 2 μl of each liposomal suspension was collected and diluted 10 times in Hepes buffer before DLS measurement. DLS measurements revealed that the average diameters of these liposomes did not change over the course of 6 hours at 75°C (fig. S1G), suggesting that liposomes composed of these synthetic lipids were thermally stable over the timeframe required for leakage experiments.

CF leakage experiment

The liposome stock solution obtained after gel filtration was first diluted 100 times in PBS (1×, pH 7.4) to prepare 5 ml of solution A. Then, solution A was diluted 10 times in PBS (1×, pH 7.4), and the resulting solution (18 ml) was aliquoted into a 0.5-ml Protein LoBind Eppendorf tube (0.3 ml per tube). For each temperature (22°, 37°, 50°, 60°, and 70°C), 11 tubes corresponding to 11 time points were prepared and incubated at the corresponding temperatures. For every time point (t = 0, 0.5, 1, 1.5, 2, 3, 4, 5, 6, 7, and 8 hours), the fluorescence (λ_{Em}: 485 nm and λ_{Ex}: 517 nm) of one tube/temperature was measured at room temperature in triplicate using a PerkinElmer EnSpire multimode plate reader and Costar 96-well half-area plates. Solution A was also diluted 10-fold in a solution of 0.5% Triton X-100 in PBS (1×, pH 7.4) to induce 100% leakage. After 15 min of incubation at room temperature, the fluorescence of the solution was measured as above. In addition, the values were corrected for the quenching of CF fluorescence by Triton X-100 using our plate reader (measured correction factor = 1.28). This leakage experiment was repeated at least three times per stock solution of liposome to ensure accuracy.

For each assay, the percent leakage ($\%_{leakage}$) was normalized using Eq. 1, where F_0 represents fluorescence at t_0, F_t represents fluorescence measurements at different times t, and F_{triton} is the fluorescence measurement of the liposome solution including Triton X-100

$$\%_{leakage} = \left(\frac{(F_t - F_0)}{(F_{triton} - F_0)}\right) \times 100 \quad (1)$$

Kinetic analysis

We used Eq. 2 to determine the rates of CF leakage at different temperatures by combining individual measurements using GraphPad Prism 5 software. The permeability coefficient of all three lipids at different temperatures was also estimated from the rates of CF leakage using Fick's law (fig. S3) (*30*)

$$\ln(\%_{leakage}) = -kt \quad (2)$$

To determine the activation free energy of CF crossing the membrane, we first needed to develop a physical model for the leakage process. We assumed a model where, in the initial state, all the CF is contained in liposomes of total volume V_l in a solution with volume V_s. The passage of CF across the membrane was assumed to be a reversible first-order process, and the time course of CF passing through the membrane and entering the system is

$$C_s = (100\%) \times \left[1 - \exp\left[-\frac{V_{tot}}{V_l} kt\right]\right] \quad (3)$$

where C_s is the CF concentration in solution (normalized between 0 and 100% to match the experimental data), the total volume is $V_{tot} = V_l + V_s$, and k is the rate constant for leakage. The volume fraction of liposome (V_l/V_{tot}) could not be exactly determined experimentally, but we could assume that it was consistent between experiments and, thus, absorb this term into the rate constant k without any loss of generality.

To relate this rate constant to the activation free energy, we make use of the Eyring-Polanyi equation (Eq. 4)

$$k = \frac{k_B T}{h} e^{\frac{\Delta S^{\ddagger}}{R}} e^{\frac{\Delta H^{\ddagger}}{RT}} \quad (4)$$

where we have split the free energy into its enthalpic and entropic components. This formula for k was inserted in the kinetic equation for C_s, and the resulting expression was used to fit the time course of leakage for each lipid. Using a maximum likelihood estimator, we simultaneously fit across all temperatures to determine $\Delta H^{\ddagger}$ and $\Delta S^{\ddagger}$ for each lipid. Nonlinear fitting procedures can be strongly influenced by outliers; however, we performed a weighted fitting procedure using the inverse variance of the data at a given time/temperature point, and this resulted in residuals that were normally distributed. All analysis was performed using R (www.R-project.org).

MD calculations of membrane properties

Structural models for the synthetic lipids were constructed and minimized using Maestro (Schrödinger LLC, New York, NY). The modeled lipids all had an extended conformation along the hydrocarbon chain. The single lipid was then translated and rotated along X and Y directions to build an initial model membrane system comprising 81 lipids. After equilibration simulations (50 ns) of this smaller membrane model, the equilibrated small membrane model was replicated along the X and Y axes to build a bigger membrane model of 729 total lipids (1458 in the case of U16). The dimensions of the bigger membrane models were in the range of 200 × 200 × 50 Å on average across the different membrane models. VMD (*31*) was used to make the translations and rotations of lipid in building the membrane. Membrane simulations of 100-ns duration were performed with NAMD (*32*), using the TIP3P explicit water model, after equilibration at temperatures of 300, 315, and 330 K, and the pressure was maintained using the Nosé-Hoover Langevin piston method at 1 atm. The temperature was maintained with the Nose-Hoover chain method, and the pressure was maintained at 1 atm. The CHARMM36 lipid force field was used with a 10 Å cutoff for van der Waals with an 8.5 Å switching distance and particle mesh Ewald for long-range electrostatics. Post-simulation trajectory analyses were carried out using R (www.R-project.org). The diffusion constants D_1 and D_2 were

determined by fitting the mean square displacement according to the formula (*33*)

$$\langle x(t)^2 \rangle = \frac{4D_1 t r_0^2}{r_0^2 + 4D_1 t} + 4D_2 t \quad (5)$$

Calculation of torsional entropy

The entropy S_i associated with torsion angle ϕ_i is given by

$$S_i = -R\int \rho(\phi_i) \ln\rho(\phi_i) d\phi_i \quad (6)$$

where R is the gas constant and $\rho(\phi_i)$ is the probability density over ϕ_i from an MD simulation—essentially, a normalized histogram of the torsion. The total first-order entropy (*20*) of one lipid molecule is computed as

$$S^1 = \sum_{i=1}^{N_{tors}} S_i \quad (7)$$

where N_{tors} is the number of torsions considered. Additional MD simulations (Fig. 4) were carried out to compute these quantities in the presence and absence of CF tethered partway through one leaflet (top or upper) of membranes made of tethered and untethered lipids. Simulations were run for T32 and U16 membrane systems, for 400 ns at a temperature of 300 K with and without CF (−2 charge state). For the simulations with CF, the molecule was constrained to remain at the plane of the membrane defined by the mean z coordinate of carbon C117 in each lipid (as shown in fig. S10), where we considered the membrane to lie in the xy plane. We analyzed the 26 torsional angles in the lipid main chains (for the 26 carbon atoms located in the center of the membrane for the unbranched methylene chain and phytanyl chain), 13 torsional angles in the top (where CF is located), and another 13 angles in the bottom. For the monolayer, T32, these are all in one molecule. For the bilayer-forming lipid U16, they are in different molecules. The T32 and U16 membranes were of essentially the same size, comprising 64 T32 molecules or 128 U16 molecules.

SUPPLEMENTARY MATERIALS

Supplementary material for this article is available at http://advances.sciencemag.org/cgi/content/full/5/5/eaaw4783/DC1

Fig. S1. Synthesis and characterization of archaea-inspired lipids.
Fig. S2. Liposome radius distribution.
Fig. S3. Time dependence of CF leakage at different temperatures for ~80-nm liposomes.
Fig. S4. Temperature-dependent CF release profile from liposomes ~200 nm in diameter.
Fig. S5. Cross-sectional views of simulated membranes.
Fig. S6. Experimental and simulated measurements of membrane thickness.
Fig. S7. Self-diffusion and lateral diffusion of lipids in simulated membranes.
Fig. S8. Area per head group in simulated membranes.
Fig. S9. Correlation plots for the variance in area per lipid.
Fig. S10. Structures of U16 and T32 lipids including the position of C117 for each lipid.

REFERENCES AND NOTES

1. L. J. Rothschild, R. L. Mancinelli, Life in extreme environments. *Nature* **409**, 1092–1101 (2001).
2. D. L. Valentine, Adaptations to energy stress dictate the ecology and evolution of the Archaea. *Nat. Rev. Microbiol.* **5**, 316–323 (2007).
3. H. Komatsu, P. L.-G. Chong, Low permeability of liposomal membranes composed of bipolar tetraether lipids from thermoacidophilic archaebacterium *Sulfolobus acidocaldarius*. *Biochemistry* **37**, 107–115 (1998).
4. E. L. Chang, Unusual thermal stability of liposomes made from bipolar tetraether lipids. *Biochem. Biophys. Res. Commun.* **202**, 673–679 (1994).
5. M. De Rosa, A. Gambacorta, B. Nicolaus, B. Chappe, P. Albrecht, Isoprenoid ethers; backbone of complex lipids of the archaebacterium *Sulfolobus solfataricus*. *Biochim. Biophys. Acta Lipids Lipid Metab.* **753**, 249–256 (1983).
6. Y. Koga, Thermal adaptation of the archaeal and bacterial lipid membranes. *Archaea* **2012**, 789652 (2012).
7. S. F. Gilmore, A. I. Yao, Z. Tietel, T. Kind, M. T. Facciotti, A. N. Parikh, Role of squalene in the organization of monolayers derived from lipid extracts of *Halobacterium salinarum*. *Langmuir* **29**, 7922–7930 (2013).
8. T. Koyanagi, G. Leriche, A. Yep, D. Onofrei, G. P. Holland, M. Mayer, J. Yang, Effect of headgroups on small-ion permeability across archaea-inspired tetraether lipid membranes. *Chem. Eur. J.* **22**, 8074–8077 (2016).
9. T. Koyanagi, G. Leriche, D. Onofrei, G. P. Holland, M. Mayer, J. Yang, Cyclohexane rings reduce membrane permeability to small ions in archaea-inspired tetraether lipids. *Angew. Chem. Int. Ed.* **55**, 1890–1893 (2016).
10. T. B. H. Schroeder, G. Leriche, T. Koyanagi, M. A. Johnson, K. N. Haengel, O. M. Eggenberger, C. L. Wang, Y. H. Kim, K. Diraviyam, D. Sept, J. Yang, M. Mayer, Effects of lipid tethering in extremophile-inspired membranes on H^+/OH^- flux at room temperature. *Biophys. J.* **110**, 2430–2440 (2016).
11. E. S. Boyd, T. L. Hamilton, J. Wang, L. He, C. L. Zhang, The role of tetraether lipid composition in the adaptation of thermophilic archaea to acidity. *Front. Microbiol.* **4**, 62 (2013).
12. G. D. Sprott, M. Meloche, J. C. Richards, Proportions of diether, macrocyclic diether, and tetraether lipids in Methanococcus jannaschii grown at different temperatures. *J. Bacteriol.* **173**, 3907–3910 (1991).
13. Y. Matsuno, A. Sugai, H. Higashibata, W. Fukuda, K. Ueda, I. Uda, I. Sato, T. Itoh, T. Imanaka, S. Fujiwara, Effect of growth temperature and growth phase on the lipid composition of the archaeal membrane from *Thermococcus kodakaraensis*. *Biosci. Biotechnol. Biochem.* **73**, 104–108 (2009).
14. D. Lai, J. R. Springstead, H. G. Monbouquette, Effect of growth temperature on ether lipid biochemistry in *Archaeoglobus fulgidus*. *Extremophiles* **12**, 271–278 (2008).
15. K. Arakawa, T. Eguchi, K. Kakinuma, Highly thermostable liposome from 72-membered macrocyclic tetraether lipid: Importance of 72-membered lipid for archaea to thrive under hyperthermal environments. *Chem. Lett.* **30**, 440–441 (2001).
16. K. Arakawa, T. Eguchi, K. Kakinuma, 36-Membered macrocyclic diether lipid is advantageous for archaea to thrive under the extreme thermal environments. *Bull. Chem. Soc. Jpn.* **74**, 347–356 (2001).
17. K. A. Connors, *Chemical Kinetics: The Study of Reaction Rates in Solution* (John Wiley & Sons,1990).
18. J. F. Nagle, H. L. Scott Jr., Lateral compressibility of lipid mono- and bilayers. Theory of membrane permeability. *Biochim. Biophys. Acta Biomembr.* **513**, 236–243 (1978).
19. J. F. Nagle, J. C. Mathai, M. L. Zeidel, S. Tristram-Nagle, Theory of passive permeability through lipid bilayers. *J. Gen. Physiol.* **131**, 77–85 (2008).
20. B. J. Killian, J. Yundenfreund Kravitz, M. K. Gilson, Extraction of configurational entropy from molecular simulations via an expansion approximation. *J. Chem. Phys.* **127**, 024107 (2007).
21. A. Finkelstein, A. Cass, Permeability and electrical properties of thin lipid membranes. *J. Gen. Physiol.* **52**, 145–172 (1968).
22. J. J. Hoyt, M. Asta, B. Sadigh, Test of the universal scaling law for the diffusion coefficient in liquid metals. *Phys. Rev. Lett.* **85**, 594–597 (2000).
23. I. Yokoyama, S. Tsuchiya, Excess entropy, diffusion coefficient, viscosity coefficient and surface tension of liquid simple metals from diffraction data. *Mater. Trans.* **43**, 67–72 (2002).
24. M. Dzugutov, A universal scaling law for atomic diffusion in condensed matter. *Nature* **381**, 137–139 (1996).
25. T. Eguchi, K. Ibaragi, K. Kakinuma, Total synthesis of archaeal 72-membered macrocyclic tetraether lipids. *J. Org. Chem.* **63**, 2689–2698 (1998).
26. S. Ohki, *Cell and Model Membrane Interactions* (Plenum Press, 1991).
27. K. Jacobson, D. Papahadjopoulos, Effect of a phase transition on the binding of 1-anilino-8-naphthalenesulfonate to phospholipid membranes. *Biophys. J.* **16**, 549–560 (1976).
28. C. A. Gobrogge, H. S. Blanchard, R. A. Walker, Temperature-dependent partitioning of coumarin 152 in phosphatidylcholine lipid bilayers. *J. Phys. Chem. B* **121**, 4061–4070 (2017).
29. A. Blicher, K. Wodzinska, M. Fidorra, M. Winterhalter, T. Heimburg, The temperature dependence of lipid membrane permeability, its quantized nature, and the influence of anesthetics. *Biophys. J.* **96**, 4581–4591 (2009).
30. L. Clary, G. Verderone, C. Santaella, P. Vierling, Membrane permeability and stability of liposomes made from highly fluorinated double-chain phosphocholines derived from diaminopropanol, serine or ethanolamine. *Biochim. Biophys. Acta Biomembr.* **1328**, 55–64 (1997).
31. W. Humphrey, A. Dalke, K. Schulten, VMD: Visual molecular dynamics. *J. Mol. Graph.* **14**, 33–38 (1996).

32. J. C. Phillips, R. Braun, W. Wang, J. Gumbart, E. Tajkhorshid, E. Villa, C. Chipot, R. D. Skeel, L. Kalé, K. Schulten, Scalable molecular dynamics with NAMD. *J. Comput. Chem.* **26**, 1781–1802 (2005).
33. J. Wohlert, O. Edholm, Dynamics in atomistic simulations of phospholipid membranes: Nuclear magnetic resonance relaxation rates and lateral diffusion. *J. Chem. Phys.* **125**, 204703 (2006).
34. D. A. Case, V. Babin, J.T. Berryman, R. M. Betz, Q. Cai, D. S. Cerutti, T. E. Cheatham III, T. A. Darden, R. E. Duke, H. Gohlke, A. W. Goetz, S. Gusarov, N. Homeyer, P. Janowski, J. Kaus, I. Kolossváry, A. Kovalenko, T. S. Lee, S. LeGrand, T. Luchko, R. Luo, B. Madej, K. Merz, F. Paesani, D. R. Roe, A. Roitberg, C. Sagui, R. Salomon-Ferrer, Gustavo de Miranda Seabra, C. Simmerling, W. Smith, J. M. Swails, R.C. Walker, J. Wang, R.M. Wolf, X. Wu, P.A. Kollman, AMBER 14 (University of California, San Francisco, 2014).
35. J. Wang, R. M. Wolf, J. W. Caldwell, P. A. Kollman, D. A. Case, Development and testing of a general amber force field. *J. Comput. Chem.* **25**, 1157–1174 (2004).
36. C. J. Dickson, B. D. Madej, Å. A. Skjevik, R. M. Betz, K. Teigen, I. R. Gould, R. C. Walker, Lipid14: The amber lipid force field. *J. Chem. Theory Comput.* **10**, 865–879 (2014).

Acknowledgments
Funding: We acknowledge the financial support from the Air Force Office of Scientific Research (FA9550-12-1-0435 and FA9550-17-1-0282). This work was also supported, in part, by the National Institute of General Medical Sciences, NIH (grant GM061300 to M.K.G.). The contents of this publication are solely the responsibility of the authors and do not necessarily represent the official views of the NIH. **Author contributions:** Y.H.K., G.L., T.K., A.G., and J.Y. planned the study, designed the leakage experiments, and analyzed the results. D.O. and G.P.H. conducted DSC measurements. J.P. and N.G. conducted cryo-EM experiments. K.D., K.G., M.K.G., and D.S. designed the computational study and analyzed the results. G.L. M.K.G., M.M., D.S., and J.Y. wrote the manuscript. **Competing interests:** M.K.G. has an equity interest in, and is a cofounder and scientific advisor of, VeraChem LLC. All other authors declare that they have no competing financial and nonfinancial interests. **Data and materials availability:** All data needed to evaluate the conclusions in the paper are present in the paper and/or the Supplementary Materials. Additional data related to this paper may be requested from the authors.

Submitted 23 December 2018
Accepted 14 March 2019
Published 1 May 2019
10.1126/sciadv.aaw4783

Citation: Y. H. Kim, G. Leriche, K. Diraviyam, T. Koyanagi, K. Gao, D. Onofrei, J. Patterson, A. Guha, N. Gianneschi, G. P. Holland, M. K. Gilson, M. Mayer, D. Sept, J. Yang, Entropic effects enable life at extreme temperatures. *Sci. Adv.* **5**, eaaw4783 (2019).

Science Advances

Entropic effects enable life at extreme temperatures

Young Hun Kim, Geoffray Leriche, Karthik Diraviyam, Takaoki Koyanagi, Kaifu Gao, David Onofrei, Joseph Patterson, Anirvan Guha, Nathan Gianneschi, Gregory P. Holland, Michael K. Gilson, Michael Mayer, David Sept and Jerry Yang

Sci Adv **5** (5), eaaw4783.
DOI: 10.1126/sciadv.aaw4783

Science Advances (ISSN 2375-2548) is published by the American Association for the Advancement of Science, 1200 New York Avenue NW, Washington, DC 20005. The title *Science Advances* is a registered trademark of AAAS.